Low-frequency gaps in a phononic crystal constituted of cylindrical dots deposited on a thin homogeneous plate

Y. Pennec, B. Djafari-Rouhani, H. Larabi, J. O. Vasseur, and A. C. Hladky-Hennion
Institut d'Electronique de Microélectronique et de Nanotechnologie, UMR CNRS 8520, Cité Scientifique, 59652 Villeneuve d'Ascq Cedex, France

(Received 13 June 2008; revised manuscript received 4 August 2008; published 5 September 2008)

We investigate theoretically the band structure of a phononic crystal of finite thickness constituted of a periodical array of cylindrical dots deposited on a thin plate of a homogeneous material. We show that this structure can display a low-frequency gap, as compared to the acoustic wavelengths in the constituent materials, similarly to the case of locally resonant structures. The opening of this gap requires an appropriate choice of the geometrical parameters, and in particular the thickness of the homogeneous plate and the height of the dots. However, the gap persists for various combinations of the materials constituting the plate and the dots. Besides, the band structure can exhibit one or more higher gaps whose number increases with the height of the cylinders. We discuss the condition to realize waveguiding through a linear defect inside the phononic crystal dots. The numerical simulations are performed by using the finite difference time domain and the finite element methods.

DOI: 10.1103/PhysRevB.78.104105 PACS number(s): 43.20.+g, 43.40.+s, 63.20.−e

I. INTRODUCTION

Over the past decade, a great deal of works has been devoted to the study of phononic crystals constituted by a periodical repetition of inclusions in a matrix background.[1] These materials have found several potential applications associated with their possibility of exhibiting absolute band gaps,[2–5] in particular in the field of confinement, wave guiding, and filtering[6–10] (analogously to their photonic counterpart), as well as in the field of sound isolation.[11–16] The band gaps may originate from the Bragg reflections resulting from the periodicity of the structure or may be due to the existence of local resonances in each unit cell. Several works have also been devoted to the study of surface modes in semi-infinite two-dimensional (2D) phononic crystals,[17–21] whereas the case of three-dimensional (3D) phononic crystals has only been dealt very recently.[22] During the last few years, a few works have also investigated the dispersion curves of acoustic waves in a free or supported plate for one-dimensional (1D) (Refs. 23–25) or 2D (Refs. 26–31) phononic crystals. The existence of band gaps in such geometries may be useful for the purpose of introducing functionalities such as waveguiding and filtering in integrated structures. They can operate at the frequencies of telecommunications (about 1 GHz) when the thickness of the plate is in the micron range. Let us also mention two recent experiments dealing with the study of vibrations in a periodical array of dots deposited on a substrate in the gigahertz regime.[32,33]

In this paper, we are dealing with the band structure in a new finite-thickness structure constituted by a square array of cylindrical dots deposited on a thin homogeneous plate. The effect observed in this geometry is the possibility of finding a low-frequency gap, which means a frequency at which the wavelengths in the constituting materials are much longer than the typical lengths in the structure such as the period of the lattice or the thickness of the plate. The opening of this gap results from a sharp bending of the dispersion curves at a given frequency. We shall discuss the existence and evolution of this gap as a function of the geometrical parameters of the structure and the material parameters of the two constituents, namely, the dots and the plate. The band structure can also display one or more higher gaps, which will be also investigated. Finally, we show the possibility of confinement and waveguiding when a guide is created inside the phononic crystal by removing or modifying a row of dots. The calculations presented in this paper are based on both the finite difference time domain (FDTD) and the finite element (FE) methods.

II. MODEL AND METHOD OF CALCULATION

As shown in Fig. 1, the physical model considered is a square lattice of cylindrical dots deposited on a plate. The z axis is chosen to be perpendicular to the plate and parallel to the cylinders axis. The lattice parameter a of the phononic crystal is chosen to be $a=1$ mm except if stated otherwise. The filling factor is defined as $\beta=\pi r^2/a^2$, where r represents the radius of the cylinders. The height of the cylinders is denoted by h and the thickness of the plate is denoted by e.

The materials constituting the dots and the plate (which are taken in most of the numerical calculations to be steel

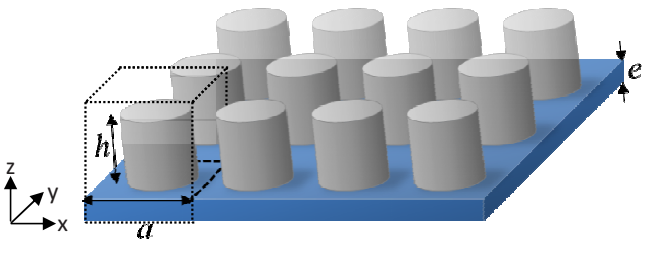

FIG. 1. (Color online) Schematic view of a phononic crystal made of a square lattice of finite cylinders deposited on a homogeneous plate. The lattice parameter is denoted as a, the height of the cylinder is denoted as h, and the thickness of the plate is denoted as e. The dashed cube ($axaxb$) represents one unit cell of the periodic structure.

TABLE I. Physical characteristics of the used materials: ρ is the density, C_{11}, and C_{12} and C_{44} are the three independent elastic moduli of cubic structure.

Constant	Silicon	Steel	Tungsten	Aluminum	Epoxy
ρ (kg/m^3)	2331	5825	18700	2730	1142
C_{11} (N/m^2)	16.57×10^{10}	26.4×10^{10}	50.23×10^{10}	10.82×10^{10}	0.754×10^{10}
C_{12} (N/m^2)	6.39×10^{10}	10.2×10^{10}	20.27×10^{10}	5.12×10^{10}	$C_{12}=C_{11}-2C_{44}$
C_{44} (N/m^2)	7.962×10^{10}	8.10×10^{10}	14.98×10^{10}	2.85×10^{10}	0.148×10^{10}

and silicon) are assumed to be isotropic or of cubic symmetry with their crystallographic axes oriented along the coordinate axes x, y, and z. The elastic constants and mass densities of the materials involved in the calculations are given in Table I.

The band structures were computed using the finite difference time domain method, which has been proven in previous works[12,34] to be an efficient method for obtaining the dispersion curves in phononic crystals. This method solves the elastic wave equations by discretizing time and space and by replacing derivatives by finite differences. Dispersion curves were calculated by using a three-dimensional unit cell (see dashed lines in Fig. 1), with dimensions ($axaxb$) which is repeated in the three directions of space, and by using the Bloch theorem, which introduces the wave vector $\boldsymbol{k}$. In the z direction, the length of the unit cell, b, is chosen in such a way as to embed the plate and the cylinder as well as a thin layer of vacuum on both sides in order to decouple the interaction between neighboring cells. Therefore, with respect to the wave vector k_z along z, the dispersion curves are flat and the calculation can be limited to $k_z=0$. The space is discretized in x, y, and z directions using a mesh interval equal to $\Delta x=\Delta y=\Delta z=a/30$. The equations of elasticity are solved with a time integration step $\Delta t=\Delta x/(4c_l)$, where c_l is the highest longitudinal velocity involving in the structure. The number of time step in general equal to 2^{19}, which is the necessary tested time for a good convergence of the numerical calculation. For each value of the wave vector (k_x,k_y) parallel to the plate, an initial random displacement is applied inside the unit cell at the origin of time. Then, the displacement field is recorded at every position in the unit cell as a function of time and finally Fourier transformed to obtain the eigenmodes of the structure for the chosen wave vector. Therefore, the band structures are rendered in terms of frequency as a function of the wave vector and plotted along the principal directions of the 2D irreducible Brillouin zone (BZ).

In order to test the convergence of the numerical simulations, some of the dispersion curves have also been calculated using the finite element method, with the help of the ATILA code.[35] Another advantage of this software is to be well adapted to display the deformation of the structure for some selected modes (see Fig. 6). In the model, only one unit cell is meshed, thanks to the Bloch-Floquet relations. A three-dimensional mesh is used and the structure is supposed to be infinite and periodic in the two directions x and y. A phase relation is applied on the lateral faces of the mesh, defining boundary conditions between adjacent cells. This phase relation is related to the wave number of the incident wave in the periodic structure. By varying the wave vector in the first Brillouin zone, the calculation gives the eigenfrequencies and the corresponding eigenvectors, related to the displacement field of the mode.

III. RESULTS AND DISCUSSION

We have made the calculation of the band structure for the system described in Fig. 1 with a propagation in the (x,y) plane, along the high-symmetry axes of the first BZ. The following parameters are used: filling factor $\beta=0.564$, height of the cylinders $h=0.6$ mm, and thickness of the plate $e=0.1$ mm. The band structure is presented Fig. 2(a) in the frequency range (0–2500 kHz) and magnified in Fig. 2(b) for its lowest part (0–400 kHz). The choice of the geometrical parameters insures the existence of two absolute band gaps extending, respectively, from 265 to 327 kHz and from 1280 to 2110 kHz. The direction XM of the BZ does not change the existence and the width of the gaps and will not been drawn in the rest of the paper so as to reduce the representations of the figures of dispersion. It should be noticed that the lowest band gap happens in a frequency range where the smallest wavelength in the constituent materials is ten times larger than the period of the phononic crystal. In the vicinity of the BZ center, the three lowest branches 1, 2, and 3, starting at Γ point, are quite similar to those of a homogeneous slab. They, respectively, correspond to the antisymmetric Lamb mode (A_0), the shear horizontal (SH) mode, and the symmetric Lamb mode (S_0). In the aim of testing the convergence of the FDTD method, dispersion curves calculation of Fig. 2 has also been performed using the finite element method. The comparison of the results presents a good agreement except for the flat band at 1280 kHz, which does not exist in the finite element method. This discrepancy does not affect the conclusions of the paper.

A. Behavior of the low-frequency gap

The behavior of the band structure of Fig. 2(b) has been studied as a function of the geometrical parameters h, e, and β for the high-symmetry axes ΓX and ΓM of the irreducible BZ (Figs. 3–5).

First, in Fig. 3, we fix the value of the filling fraction ($\beta=0.564$) and the thickness of the plate ($e=0.1$ mm) while increasing the height h of the dots. For a small thickness $h=0.1$ mm [Fig. 3(a)] the band structure does not display any band gap in the range (0–1200 kHz) although one can notice a bending of both shear horizontal mode (branch 2) and more particularly of symmetric Lamb mode, which becomes a

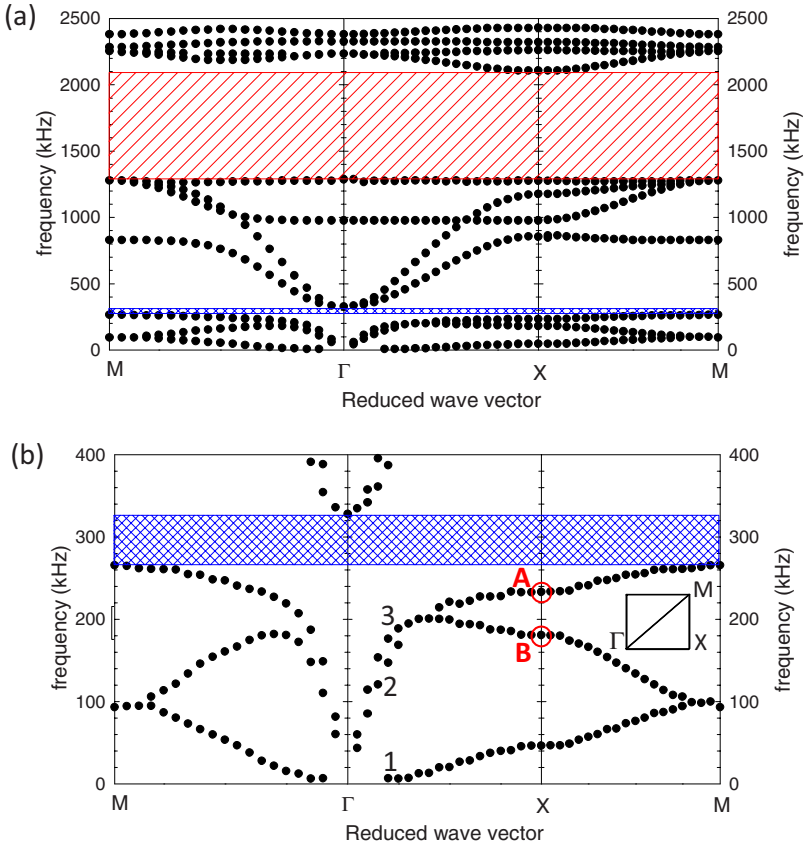

FIG. 2. (Color online) (a) Band structure in the frequency range (0–2500 kHz) of the model of Fig. 1 for steel cylinders on a silicon plate, calculated in the first irreducible BZ of the phononic crystal. The lattice parameter is $a=1$ mm ($\beta=56.4\%$), the height of the cylinders $h=0.6$ mm, and the thickness of the plate $e=0.1$ mm. (b) Same as (a) in the magnified frequency range (0–400 kHz). Points A and B correspond, respectively, to the extremities of branches 2 and 3 at the X point of the Brillouin zone.

negative slope branch (branch 3). Increasing the height of the cylinders from 0.1 to 0.2 mm [Fig. 3(b)], the first three dispersion curves shift downward and the band structure shows the opening of a small absolute gap in the range (675.5–695.2 kHz), which results from a most important bending of the shear horizontal mode (branch 2). With increasing h, the dispersion curves continue to shift downward. Until $h=0.6$ mm, the central frequency of the first gap decreases and its width becomes larger [Fig. 3(c)]. Increasing further h, one can notice a slower decrease in point B, situated at the boundary X of the BZ on branch 3, with respect to the other branch extremities, leading to the closing of the gap. This occurs first in the ΓM direction for $h>1.0$ mm and then in both directions of the BZ as seen for example in Fig. 3(d) for $h=2.7$ mm in the magnified frequency range (0–300 kHz).

Figure 4 presents the evolution of the dispersion curves as a function of the thickness of the plate for constant values of $\beta=0.564$ and $h=0.6$ mm. Increasing e from 0.1 to 0.4 mm, the dispersion curves shift to higher frequencies and the gap closes first in the ΓM direction [Fig. 4(b)] and finally in both directions of the BZ as sketched in Fig. 4(c) for $e=0.6$ mm. This result is due to a faster upward shift of point B with respect to the other branch boundaries.

On the basis of a closed gap ($e=0.4$ mm), we show in Fig. 5 the influence of the filling factor β on the dispersion curves. The reduction of the filling factor is obtained by increasing the lattice parameter a from 1.0 to 1.6 mm, keeping constant all the other parameters of the structure ($r=0.42$ mm, $e=0.4$ mm, and $h=0.6$ mm). In Fig. 5(a), with $a=1.0$ mm, the gap is closed in the ΓM direction of the BZ. Increasing a to 1.2 mm, the dispersion curves move downward and the gap appears in the frequency range (765.1–778.9 kHz) [Fig. 5(b)]. This result comes from a faster downward shift of point B', situated at the boundary M of the BZ on branch 3, with respect to the other branch boundaries as seen in the ΓM direction of Fig. 5(c).

To summarize the above trends, the low-frequency gap is generated from the bending of both shear horizontal (branch 2) and symmetric Lamb mode (branch 3) of the plate. Since the extremities A and B of these branches move differently (although in the same direction) with the geometric parameters e/a and h/a, the opening of the gap requires an appropriate choice of these parameters. In all cases, the opening of the gap is closely linked to the shift and bending of branch 3 and, for small h [Fig. 3(a)], to the shift and bending of branch 2. In comparison with the other band extremities, the evolution of point B is most importantly related to the thickness of the plate and the lattice parameter rather than to the height of the dots. The central frequency of the gap depends upon all the geometrical parameters e, h, and a. It decreases either by increasing h, decreasing e, or increasing a.

We have investigated the spatial distribution of the eigenmodes inside the unit cell for the modes A and B situated at the extremities of branches 2 and 3 in Fig. 2(b), in which bending is at the origin of the gap. The parameters are $h=0.6$ mm, $e=0.1$ mm, and $\beta=56.4\%$. Calculations were performed with the help of the finite element method using ATILA® code,[35] which is well adapted to sketch the deformation of the structure. The initial excitation of the mode is made in the ΓX direction. The results for mode A [wave vector $\boldsymbol{k}_A=(\pi/a,0,0)$ and frequency $f_A=233.0$ kHz] and mode B [$\boldsymbol{k}_B=(\pi/a,0,0)$ and frequency $f_B=180.6$ kHz] are

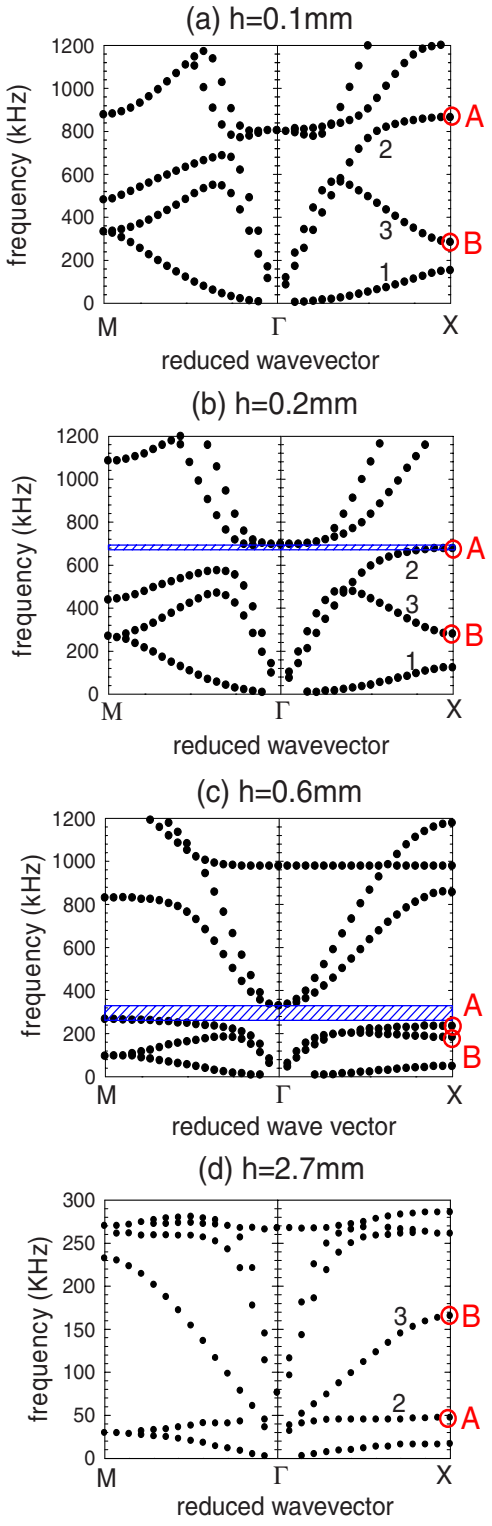

FIG. 3. (Color online) Evolution of the band structure as a function of the height of the dots, keeping constant the thickness of the plate (e=0.1 mm) and the filling factor (β=56.4%). (a) h=0.1, (b) 0.2, (c) 0.6, and (d) 2.7 mm.

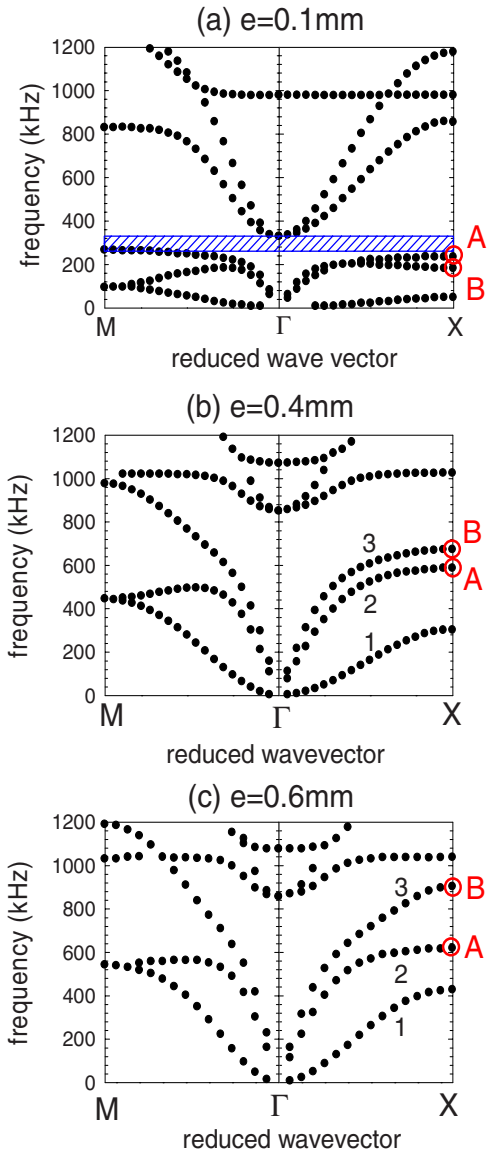

FIG. 4. (Color online) Evolution of the band structure as a function of the thickness of the plate keeping constant the height of the dots (h=0.6 mm) and the filling factor (β=56.4%). (a) e=0.1, (b) 0.4, and (c) 0.6 mm.

plotted in Figs. 6(a) and 6(b) using a cut along the (y,z) or (x,z) plane. In Fig. 6(a), the mode A is clearly associated with an oscillation of the dot in the y direction together with a weak bending of the plate. In Fig. 6(b), the vibration of the mode B involves, in the z direction, an oscillation of the dot correlated with a strong bending of the slab. In both cases, the displacement fields are distributed in the dot, as well as in the plate, in agreement with the dependence of the points A and B of the dispersion curves with all the geometrical parameters h, e, and a. More specifically, for mode A, the stronger deformation in the dot than in the plate is related to a stronger dependence of point A of the BZ with the height of the dot (seen in Fig. 3) than with the other parameters. On the contrary, for mode B, the deformation affects more the plate than the dot. This means that the motion of point B of the dispersion curve is more dependant of the thickness of the plate e and the lattice parameter a (seen in Figs. 4 and 5) than of the height h of the dot.

We have also investigated the persistence of this gap upon different combinations of the materials constituting the dot

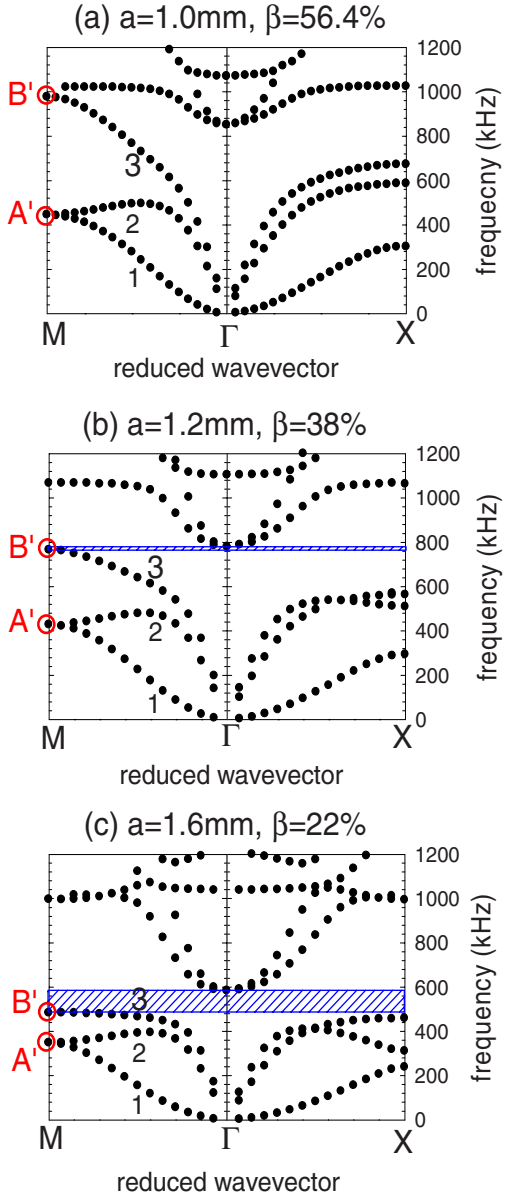

FIG. 5. (Color online) Evolution of the band structure as a function of the filling factor keeping constant the height of the dots (h =0.6 mm), the thickness of the plate (e=0.4 mm), and the radius of the cylinders (r=0.42 mm). (a) a=1 mm (β=56.4%), (b) a =1.2 mm (β=38%), and (c) a=1.6 mm (β=22%). Points A' and B' correspond, respectively, to the extremities of branches 2 and 3 at the M point of the Brillouin zone.

and the plate among a set of five materials (tungsten, steel, silicon, aluminum, and epoxy). Table I reports the densities and velocities of the constituent materials. In Fig. 7(a), we show the limits of the gap by changing the material of the plate when the dots are made of steel. Similarly, Fig. 7(b) displays the gap limits for various materials in the dots and the plate being made of silicon. One can notice the persistence of this gap even if the constituting materials are identical. This supports the origin of the gap as being related to the geometrical rather than physical parameters of the structure. On the other hand, the central frequency of the gap is very dependent upon the choice of the materials and happens

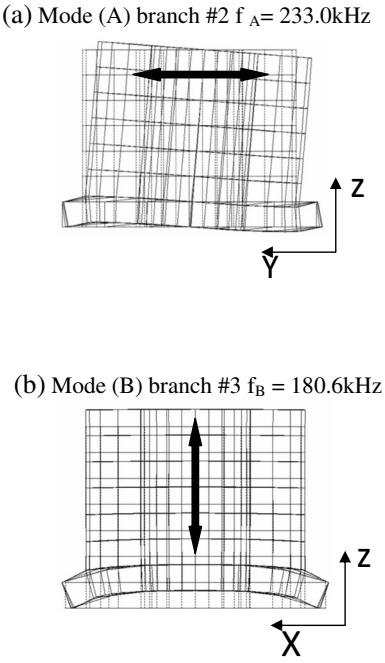

FIG. 6. Displacement fields of the modes A and B in Fig. 2(b). The dashed lines correspond to the rest position of the structure.

at lower frequencies when we combine a high-density material (steel) in the cylinders with a low-density material (epoxy) in the plate. For such a system (steel dots on epoxy plate), the gap extends from 43 to 63 kHz. It is worthwhile to notice that one can obtain a gap in the audible frequency range, around 2 kHz, for a period of a=20 mm and the other parameters being scaled accordingly. Such solid systems could then easily be used as vibrationless environment for high-precision mechanical systems.

In general phononic crystal studies,[1–5] the band gaps may originate from the Bragg reflections resulting from the periodicity of the structure. We note that the low-frequency gap reported here occurs at a frequency such that the wavelength

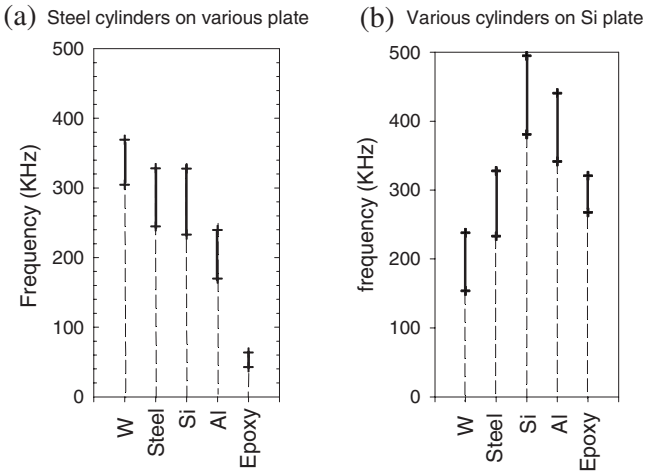

FIG. 7. Evolution of the lowest-frequency gap limits for different combinations of constituting materials. (a) Steel dots on a plate of different materials. (b) Various dots on a silicon plate. The geometrical parameters are e=0.1 mm, h=0.6 mm, and β=56.4%.

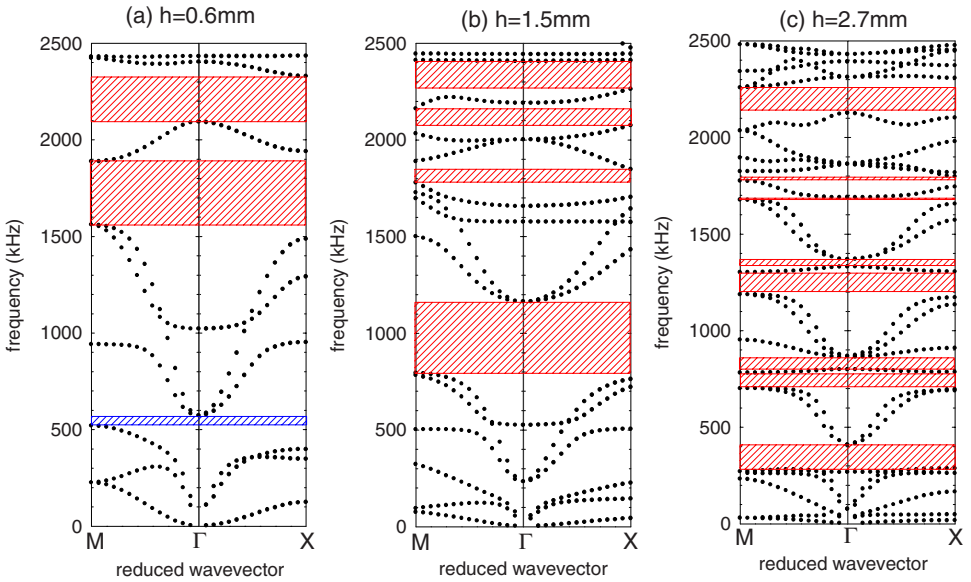

FIG. 8. (Color online) Evolution of the band structure for different values of the height of the dots: (a) $h=0.6$, (b) 1.5, and (c) 2.7 mm. The other geometrical parameters are $e=0.2$ mm and $\beta=56.4\%$.

in all constituting materials is at least one order of magnitude larger than the geometrical sizes of the structure. Thus, it shows some similarity with the behavior obtained in locally resonant sonic materials.[11–16] Still, from the spatial distribution of the displacement field, we cannot attribute a totally localized character to the modes in this frequency range. Instead, the competitive motions of branches 2 and 3 by varying the geometrical parameters should allow the opening of the gap.

B. Behavior of the higher gaps

The behavior of the higher gap observed in the band structure of Fig. 2(a) has been studied as a function of the geometrical parameters h, e, and β, along the high-symmetry axes ΓX and ΓM of the irreducible BZ (Fig. 8). We choose to refer to the thickness $e=0.2$ mm to avoid a thin discretization of the space thus decreases time of calculation.

In Fig. 8, we fix the values of the filling fraction $\beta=0.564$ and the thickness of the plate ($e=0.2$ mm) while increasing the height of the dots from $h=0.6-2.7$ mm. For $h=0.6$ mm [Fig. 8(a)], we note the existence of three gaps. The lowest one (519.3–571.7 kHz), discussed in the previous section, closes for $h>1.0$ mm. Besides, the band structure exhibits two higher gaps, respectively, in the frequency ranges (1560–1887 kHz) and (2092–2328 kHz). When increasing h to 1.5 mm [Fig. 8(b)] and then to 2.7 mm [Fig. 8(c)], the central frequencies of these gaps move downward together with the dispersion curves, whereas additional absolute band gaps appear at higher frequencies. It is interesting to remark that, up to a certain frequency range, the opening of the gaps results from the crossing of the normal acoustic branches with almost flat bands, which is similar to the case of locally resonant materials.

We have also studied the evolution of the gaps with the thickness of the plate e, keeping constant $h=2.7$ mm and $\beta=56.4\%$ [Fig. 9(a)]. Increasing e from 0.1 to 1.0 mm, we observe a slow variation of the central frequency of the gap. In addition, most of the gaps close for $e>1$ mm, due to many dispersion branches moving downward. The evolution of the gaps with the filling factor has also been investigated. When increasing a from 1.0 [Fig. 8(c)] to 1.4 mm [Fig. 9(b)] with the same h and e, several branches move downward from the high-frequency region and progressively fill the higher gaps; at the same time, the lowest remaining gaps keep their central frequencies almost preserved.

C. Propagation of guiding waves in the slab

In this section, we study the possibility of propagating a confined mode in a rectilinear waveguide created inside the

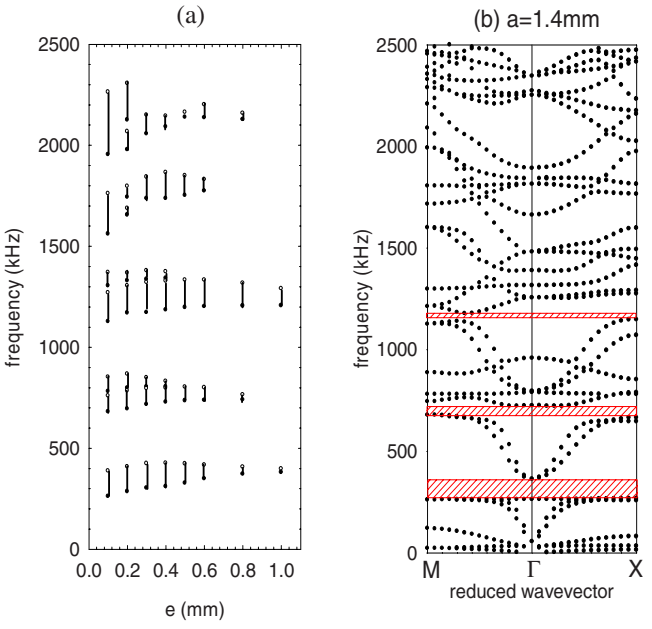

FIG. 9. (Color online) (a) Evolution of the gaps of Fig. 2(a) as a function of the thickness of the plate, keeping constant the other geometrical parameters ($h=2.7$ mm and $\beta=56.4\%$). (b) Dispersion curves for a low filling fraction $\beta=38\%$ (lattice parameter $a=1.4$ mm) and the geometrical parameters $h=2.7$ mm and $e=0.2$ mm.

phononic crystal. The geometrical parameters are the same as in Fig. 2, i.e., $\beta=56.4\%$, $h=0.6$ mm, and $e=0.1$ mm that ensures the existence of the largest forbidden gaps. The FDTD calculation is performed by using a supercell containing five unit cells in the y direction. The guide is created by removing one row of dots in the third unit cell, thus constituting a linear waveguide in the x direction. The width of the waveguide, δ, has been chosen as a variable parameter to investigate the existence and number of localized modes in the band gap.[8] Fig. 10(a) shows the band structure in the ΓX direction for the waveguide structure with $\delta=0.55a$. The dispersion curve exhibits three additional branches inside the higher gap (1287–2106 kHz) while no supplementary branches appear inside the lowest gap. Increasing the width of the waveguide leads to the lowering of the frequencies of the waveguide modes. Figure 10(b) shows the band structure for a waveguide with $\delta=1.05a$, which presents one additional mode in the lowest forbidden band (265.2–327.9 kHz). To show the confinement of such modes inside the waveguide, we focus on the points C and D of the dispersion curves. The maps of the displacement fields associated with both modes are, respectively, sketched in Figs. 10(c) and 10(d). In both cases, the acoustic field is essentially confined in the area of the waveguide and does not leak out into the rest of the structure.

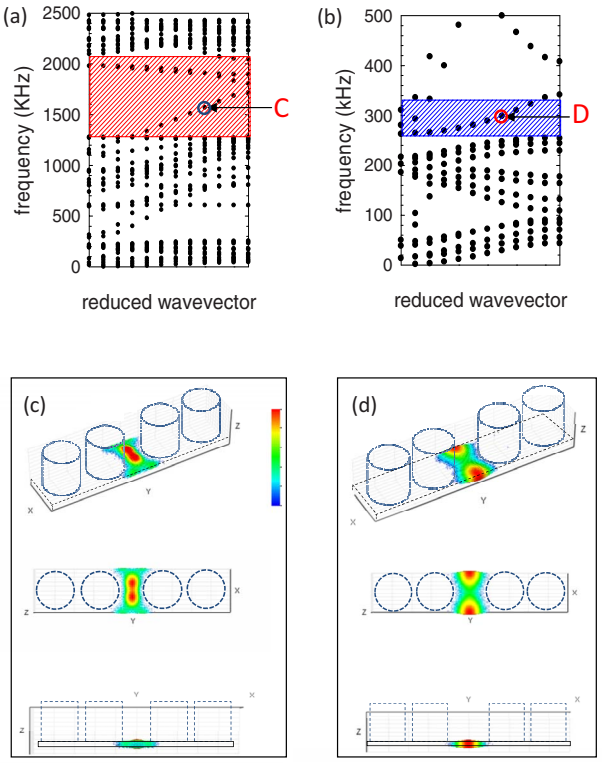

FIG. 10. (Color online) [(a)–(b)] Band structures along the ΓX direction for a phononic crystal containing a waveguide of width δ obtained by removing one row of dots. The calculation is performed with a supercell containing 1×5 unit cells and the dots are removed in the third unit cell. The blue and red hatched areas indicate the location of the absolute band gaps of the perfect structure. (a)–(b) display, respectively, the dispersion curves for a waveguide width of $\delta=0.55a$ and $\delta=1.05a$. [(c)–(d)] Maps of the modulus of the elastic displacement fields for the modes labeled C and D, represented in three-quarter, top, and lateral views. The red and blue colors, respectively, correspond to the maximum and minimum of the displacement.

IV. CONCLUSIONS

The purpose of this paper was to investigate, using the finite difference time domain and the finite element methods, the dispersion of the elastic waves of a periodic array of dots deposited on a plate. We showed the possibility of a low-frequency gap and its existing conditions as a function of the geometrical parameters in the structure and the physical parameters of the constituting materials. This gap is generated by the bending of the two plate's modes, i.e., the SH and the (S_0) modes. The central frequency of the gap depends on all geometrical parameters (thickness of the plate, the height of the dots, and the filling factor). The gap can exist for very different combinations of the constituting materials, supporting the origin of the gap as being due to the geometry of the structure. However, the central frequency and the width of the gap are dependent upon the material properties. More particularly, in view of acoustic isolation, it would be suitable to choose a high-density material for the cylinders and a low-density one for the plate. We also showed the existence of higher gaps, especially by increasing the height of the cylinders. Those gaps can also appear at low frequency for much larger values of h. Finally, we showed that plate modes can be guided inside a linear defect created by removing one row of dots. Similar studies should be performed for different shapes of the dots, hollow or coated cylinders, etc. Such system could found original application in the field of guiding and filtering waves, as well as sound isolation inside vibrating plate structures.

ACKNOWLEDGMENT

This work was supported in part by the European Commission (EC) 7th Framework Programme (FP7), under the (IP) project reference No. 216176 (NANOPACK, www.nanopack.org).

[1] For a review, see M. S. Kushwaha, Recent Res. Dev. Appl. Phys. **2**, 743 (1999).

[2] M. S. Kushwaha, P. Halevi, L. Dobrzynski, and B. Djafari-Rouhani, Phys. Rev. Lett. **71**, 2022 (1993).

[3] M. M. Sigalas and E. N. Economou, Solid State Commun. **86**, 141 (1993).

[4] F. R. Montero de Espinosa, E. Jimenez, and M. Torres, Phys. Rev. Lett. **80**, 1208 (1998).

[5] J. V. Sanchez-Pérez, D. Caballero, R. Martinez-Sala, C. Rubio, J. Sanchez-Dehesa, F. Meseguer, J. Llinares, and F. Galvez, Phys. Rev. Lett. **80**, 5325 (1998).
[6] M. Torres, F. R. Montero de Espinosa, D. Garcia-Pablos, and N. Garcia, Phys. Rev. Lett. **82**, 3054 (1999).
[7] M. Kafesaki, M. M. Sigalas, and N. Garcia, Phys. Rev. Lett. **85**, 4044 (2000); Physica B **296**, 190 (2001).
[8] A. Khelif, B. Djafari-Rouhani, J. O. Vasseur, and P. A. Deymier, Phys. Rev. B **68**, 024302 (2003).
[9] Y. Pennec, B. Djafari-Rouhani, J. O. Vasseur, A. Khelif, and P. A. Deymier, Phys. Rev. E **69**, 046608 (2004).
[10] Y. Pennec, B. Djafari-Rouhani, J. O. Vasseur, H. Larabi, A. Khelif, A. Choujaa, S. Benchabane, and V. Laude, Appl. Phys. Lett. **87**, 261912 (2005).
[11] Z. Liu, X. Zhang, Y. Mao, Y. Y. Zhu, Z. Yang, C. T. Chan, and P. Sheng, Science **289**, 1734 (2000).
[12] Ph. Lambin, A. Khelif, J. O. Vasseur, L. Dobrzynski, and B. Djafari-Rouhani, Phys. Rev. E **63**, 066605 (2001).
[13] C. Goffaux, J. Sanchez-Dehesa, A. Levy Yeyati, Ph. Lambin, A. Khelif, J. O. Vasseur, and B. Djafari-Rouhani, Phys. Rev. Lett. **88**, 225502 (2002).
[14] M. Hirsekorn, Appl. Phys. Lett. **84**, 3364 (2004).
[15] Y. A. Kosevich, C. Goffaux, and J. Sanchez-Dehesa, Phys. Rev. B **74**, 012301 (2006).
[16] H. Larabi, Y. Pennec, B. Djafari-Rouhani, and J. O. Vasseur, Phys. Rev. E **75**, 066601 (2007).
[17] Y. Tanaka and S. I. Tamura, Phys. Rev. B **58**, 7958 (1998).
[18] Y. Tanaka and S. I. Tamura, Phys. Rev. B **60**, 13294 (1999).
[19] T. T. Wu, Z. G. Huang, and S. Lin, Phys. Rev. B **69**, 094301 (2004).
[20] V. Laude, M. Wilm, S. Benchabane, and A. Khelif, Phys. Rev. E **71**, 036607 (2005).
[21] J. H. Sun and T. T. Wu, Phys. Rev. B **74**, 174305 (2006).
[22] R. Sainidou, B. Djafari-Rouhani, and J. O. Vasseur, Phys. Rev. B **77**, 094304 (2008).
[23] J. J. Chen, K. W. Zhang, J. Gao, and J. C. Cheng, Phys. Rev. B **73**, 094307 (2006).
[24] J. J. Chen, H. L. W. Chan, and J. C. Cheng, Phys. Lett. A **366**, 493 (2007).
[25] J. Gao, X. Y. Zou, J. C. Cheng, and B. W. Li, Appl. Phys. Lett. **92**, 023510 (2008).
[26] J. O. Vasseur, P. A. Deymier, B. Djafari-Rouhani, and Y. Pennec, Proceedings of the IMECE 2006, ASME International Mechanical Engineering Congress and Exposition, Chicago, Illinois, November 2006 (unpublished), pp. 5–10.
[27] J. C. Hsu and T. T. Wu, Phys. Rev. B **74**, 144303 (2006).
[28] A. Khelif, B. Aoubiza, S. Mohammadi, A. Adibi, and V. Laude, Phys. Rev. E **74**, 046610 (2006).
[29] J. O. Vasseur, A. C. Hladky-Hennion, B. Djafari-Rouhani, F. Duval, B. Dubus, and Y. Pennec, J. Appl. Phys. **101**, 114904 (2007).
[30] J. C. Hsu and T. T. Wu, Appl. Phys. Lett. **90**, 201904 (2007).
[31] J. O. Vasseur, P. A. Deymier, B. Djafari-Rouhani, Y. Pennec, and A. C. Hladky-Hennion, Phys. Rev. B **77**, 085415 (2008).
[32] J. F. Robillard, A. Devos, and I. Roch-Jeune, Phys. Rev. B **76**, 092301 (2007).
[33] C. Giannetti, B. Revaz, F. Banfi, M. Montagnese, G. Ferrini, F. Cilento, S. Maccalli, P. Vavassori, G. Oliviero, E. Bontempi, L. E. Depero, V. Metlushko, and F. Parmigiani, Phys. Rev. B **76**, 125413 (2007).
[34] Y. Tanaka, Y. Tomoyasu, and S. Tamura, Phys. Rev. B **62**, 7387 (2000).
[35] ATILA Finite Element Code for Piezoelectric and Magnetostrictive Transducers Modeling, Version 5.2.1, user's manual, ISEN, Acoustics Laboratoy, Lille France, 2002.